TOPOLOGY DESIGN OPTIMIZATION OF NANOPHOTONIC DEVICES FOR ENERGY CONCENTRATION

R. MATTOSO, L.H. GABRIELLI AND A.A. NOVOTNY*

Abstract. In this work, a novel topology optimization method for the synthesis of nanophotonic energy concentrators is proposed. The forward problem is governed by the Maxwell equations in the frequency domain. The basic idea consists in finding the best two phase material distribution that concentrates the energy in a given target domain. More precisely, a shape functional measuring the electrical energy of the system within a small region of the nanodevice is maximized with respect to silicon and glass spatial distribution by using the topological derivative method. Therefore, since the resulting optimization method is based on a scattering problem formulation, any issues that would come from eigenmode calculations are here avoided. In addition, the proposed shape functional can be properly defined both outside or overlapping the design (moving) domain itself, increasing the range of applications of the proposed approach. The associated topological gradient is rigorously derived and used to devise a simple and efficient black/white binary topology design algorithm, which naturally conforms to practical fabrication constraints for nanodevices. Finally, a set of numerical experiments are presented showing different features of the proposed approach, including its capability in selectively producing the required hot-spots within the nanodevices.

1. Introduction

Nano- and micro-fabrication technologies have enabled the development of devices built in nanometre scales. These devices are today found in applications ranging from communications and agriculture, to medicine and construction. That is because the scientific and engineering applications of nanostructured devices are equally diverse, providing cutting-edge platforms for research and development in electronics, mechanics, optics, acoustics, and many other technology fields [1].

In this work, we are interested in the design of nanostructures for applications in optics. Optical nanowires are the equivalent of optical fibers but for communications inside the chip. They are conventionally composed by two dielectric materials with distinct refractive indices. The material with high index is used as the waveguide core, which is surrounded by the low-index material, known as waveguide cladding [2, 3]. Light remains confined in the high-index material and can be guided, filtered, modulated and freely processed by linear and non-linear devices designed in the same platform. The distribution of the two materials establishing the functionality of the devices gives birth to a number of design challenges to which topology optimization methods are a successful general approach.

Many topology optimization methods have been proposed since the publication of the seminal paper by Bendsøe and Kikuchi [4], including the most used SIMP method [5]. Specifically in nano optics, topology optimization has been subject of intensive research for the last two decades and different approaches have been proposed, such as bio-inspired methods [6], pixel-by-pixel optimization [7], level-set methods [8] and transformation optics [9]. For a comprehensive overview on applications of topology optimization methods

Key words and phrases. Topology Optimization, Nanophotonic Devices, Energy Concentration, Topological Derivative Method.

in nanophotonics, see for instance [10, 11]. A recent approach which has been successfully applied in the context of design of nanophotonic devices is based on the topological derivative method [12].

The topological derivative concept was introduced in 1999 by Sokolowski & Zochowski [13]. The topological derivative represents the sensibility of a given shape functional with respect to singular domain perturbations, such as holes, inclusions, source-terms and cracks [14]. The topological derivative has been conceived to deal with structural topology optimization. More recently, it has been applied for solving varying other problems such as antenna design in hyperthermia therapy, inverse reconstruction problems, multiscale material design and fracture mechanics modelling. A detailed explanation of the topological derivative method and its applications can be found in [15] and [16], respectively.

In this paper, we are interested in the optimal design of structures that concentrate energy, such as resonators, that could be used in the fields of non-linear optics or photovoltaics, for example. Because the problem of designing a high-quality resonator is known to be ill-posed [17], we propose the use of the topological derivative method to formulate the optimization problem directly in terms of the energy density in the objective region, instead of the quality factor of the structure. The forward problem is governed by the Maxwell's equation in the frequency domain. The basic idea consists in maximizing the energy of the system within a small region of the optical device, with respect to silicon dioxide (SiO_2) and silicon (Si) distribution by using the topological derivative method. In particular, the associated topological derivative is used to devise a topology optimization algorithm specifically designed to deal with black/white material distribution. In contrast to [12] where the shape functional is concentrated far from the design domain, in this work we deal with a moving domain problem in which the shape functional is concentrated within the design domain itself, leading to a more complicated scenario from the theoretical point of view. This work presents the derivation of the sensitivity analysis for this type of problem and, using a topological derivative based optimization algorithm, shows the application of the derived equations in the optimization of nanophotonic energy concentration in a few different scenarios.

This paper is organized as follows. In Section 2, the forward problem we are dealing with is introduced. The shape functional to be minimized and its related topological derivative are discussed in Section 3. The resulting topology design algorithm based on the topological derivative and a level-set domain representation method is presented in Section 4. A set of numerical experiments showing different features of the proposed methodology is presented in Section 5. Finally, the paper ends with some concluding remarks through Section 6. For the reader convenience, the proof of the main theoretical result of the paper is relegated to the Appendix A.

2. Problem Formulation

In this section the topology optimization problem we are dealing with is presented. It consists in the design of optical devices that concentrate energy in a target region. The Maxwell's system written in the frequency domain is considered as governing equations. We want to maximize the energy of the system within a small region of the optical device, with respect to silicon dioxide (SiO_2) and silicon (Si) distribution.

More precisely, let us consider an open and bounded domain $\mathcal{D} \subset \mathbb{R}^d$, with $d = 2, 3$. A near-field domain is denoted as $\mathcal{B} \subset \mathcal{D}$. The optimization region is given by $\Omega \subset \mathcal{B}$, which is split into two disjoints subdomains Ω_1 and Ω_2, such that $\Omega = \Omega_1 \cup \Omega_2$ and $\Omega_1 \cap \Omega_2 = \varnothing$, with Ω_1 and Ω_2 representing regions with refractive indices n_1 and n_2, respectively. We also define a target domain $\omega \subset \mathcal{B}$, as illustrated in Figure 1.

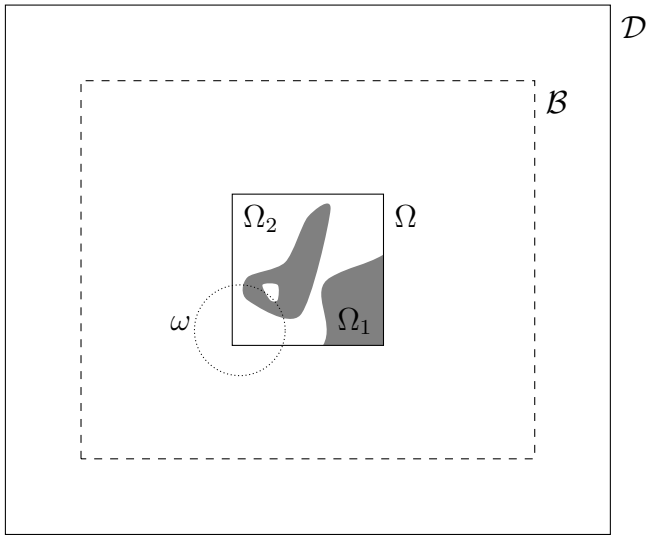

FIGURE 1. Domain definitions for the electromagnetic problem and the calculation of the topological derivative.

The weak form of the electromagnetic scattering problem is stated as follows: find $E \in \mathcal{V}$, such that

$$\int_{\mathcal{D}} \left(\nabla \times E \cdot \nabla \times W - k_0^2 n^2 E \cdot W \right) \mathrm{d}x = \int_{\mathcal{D}} Q \cdot W \mathrm{d}x \quad \forall\, W \in \mathcal{V} \tag{2.1}$$

where k_0 is the wavenumber in vacuum and n is the refractive index assumed to be a piecewise constant function. Finally, the space $\mathcal{V}$ is defined as

$$\mathcal{V} := \{W \in H_{\mathrm{curl}}(\mathcal{D}; \mathbb{C}^d) : \nu \times W = 0 \text{ on } \Gamma\}, \tag{2.2}$$

where ν is the exterior unit normal vector to $\mathcal{D}$, $H_{\mathrm{curl}}(\mathcal{D}; \mathbb{C}^d)$ is used to denote the standard complex-valued Hilbert space of vector functions $W : \mathcal{D} \mapsto \mathbb{C}^d$, such that $W \in L^2(\mathcal{D}; \mathbb{C}^d)$ and $\nabla \times W \in L^2(\mathcal{D}; \mathbb{C}^d)$. Outside $\mathcal{B}$, the formulation can be extended to include anisotropic and magnetic materials, as required when open domains are simulated with the help of a Perfectly Matched Layer (PML) approach. Finally, the electric energy density of the system can be written as

$$u(E) = k_0^2 n^2 \|E\|^2. \tag{2.3}$$

Finally, the quantity we are interested in is given by the electric energy stored in ω, namely

$$U(\omega) = \int_{\omega} k_0^2 n^2 \|E\|^2 \mathrm{d}x. \tag{2.4}$$

3. Topological Derivative Method

In this section we present the main theoretical result of the paper. It is given by the topological derivative of the shape function (2.4). The result is summarized through the following theorem:

Theorem 1. *Let us consider the shape functional $U(\omega)$ defined in* (2.4)*. Its associated topological derivative, with respect to the nucleation of a small inclusion endowed with different refractive index from the background, is given by*

$$D_{\mathcal{T}} U(\omega)(x) = (\gamma^2 - 1) k_0^2 n^2 (\|E\|^2 \chi_\omega + \Re\{E \cdot V\})(x), \tag{3.1}$$

where E is solution to equation (2.1) and χ_ω is the characteristic function of region ω, defined as

$$\chi_\omega = \begin{cases} 1, & \text{if } x \in \omega, \\ 0, & \text{if } x \notin \omega. \end{cases} \tag{3.2}$$

In addition, function V is solution to the following adjoint problem: For all $W \in \mathcal{V}$, find $V \in \mathcal{V}$, such that

$$\int_{\mathcal{D}} \left(\nabla \times V \cdot \nabla \times W - k_0^2 n^2 V \cdot W \right) \mathrm{d}x = 2 \int_\omega k_0^2 n^2 \overline{E} \cdot W \mathrm{d}x. \tag{3.3}$$

where $\overline{(\cdot)}$ is used to denote the complex conjugate of $(\cdot)$. Finally, $\gamma(x)$ is the contrast on the refractive index defined as

$$\gamma(x) = \begin{cases} \frac{n_2}{n_1}, & x \in \Omega_1, \\ \frac{n_1}{n_2}, & x \in \Omega_2, \end{cases} \tag{3.4}$$

where n_1 and n_2 are reflective index of Si and SiO_2, respectively.

Proof. The proof of this result is presented in Appendix A. □

Remark 2. *The additional term in (3.1), which follows multiplied by the characteristic function χ_ω, comes out from the contribution of the shape functional itself that is given by integral over the moving domain Ω. This term represents the main theoretical contribution with respect to [12], where the shape functional is concentrated far from the design domain.*

The goal of this work is to find a nanodevice in which the energy of the system is maximized in ω. Therefore, from (2.4), we define the energy-shape functional to be minimized as

$$\mathcal{J}(E) = -\int_\omega k_0^2 n^2 \|E\|^2 \mathrm{d}x. \tag{3.5}$$

According to Theorem 1, the topological derivative of $\mathcal{J}(E)$ defined in (3.5), with respect to the nucleation of a small inclusion endowed with different refractive index from the background, is given by

$$D_\mathcal{T} \mathcal{J}(E)(x) = -D_\mathcal{T} U(\omega)(x). \tag{3.6}$$

4. Topology Design Algorithm

Following the original ideas introduced by Amstutz & Andrä [18], in this section we present a topology design algorithm based on the topological derivative of the energy-shape functional combined with a level-set domain representation method for solving the optimization problem we are dealing with. Therefore, let $\Psi : \Omega \mapsto \mathbb{R}$ be a level-set function of the form

$$\begin{cases} \Psi(x) < 0, & \text{if } x \in \Omega_1, \\ \Psi(x) > 0, & \text{if } x \in \Omega_2. \end{cases} \tag{4.1}$$

We define the steepest descent direction g as

$$g(x) := \begin{cases} -D_\mathcal{T} \mathcal{J}(E)(x), & \text{if } \Psi(x) < 0, \\ +D_\mathcal{T} \mathcal{J}(E)(x), & \text{if } \Psi(x) > 0. \end{cases} \tag{4.2}$$

where $D_\mathcal{T} \mathcal{J}(E)$ is given by (3.6). Then, g can be written as

$$g(x) = -(n_1^2 - n_2^2) k_0^2 (\|E(x)\|^2 \chi_\omega(x) + \Re\{E(x) \cdot V(x)\}). \tag{4.3}$$

The angle θ between the level-set function Ψ and the descent direction g is given by

$$\theta = \arccos\left[\frac{\langle g, \Psi\rangle_{L^2(\Omega;\mathbb{R}^d)}}{\|g\|_{L^2(\Omega;\mathbb{R}^d)}\|\Psi\|_{L^2(\Omega;\mathbb{R}^d)}}\right], \tag{4.4}$$

so that $\theta = 0$ represents a local optimality condition, which has been rigorously derived in [19].

From these elements, a topology optimization algorithm can be devised. In particular, for a generic iteration $j \in \mathbb{N}$, the updated level-set function is governed by the following equation derived in [18, Section 3.2] with the help of Euler's scheme on a sphere and trigonometric formulas:

$$\Psi_{j+1} = \frac{1}{\sin\theta_j}\left[\sin((1-k)\theta_j)\Psi_j + \sin(k\theta_j)\frac{g_j}{\|g_j\|_{L^2(\Omega;\mathbb{R}^d)}}\right], \tag{4.5}$$

where k is a step size determined by a line-search procedure in order to decrease the value of the shape functional. The algorithm is initialized by setting $\Psi_0 = -1$ or $\Psi_0 = 1$ for the whole optimization region, or any spatial distribution of these two values. The process ends when the condition $\theta_j < \epsilon_\theta$ is satisfied at some iteration j, where ϵ_θ is a given small numerical tolerance. If k is found to be smaller then a given numerical tolerance ϵ_k and the local optimality condition is not yet satisfied, namely $\theta_j > \epsilon_\theta$, then a mesh refinement of the domain is carried out in order to increase the set of possible local minima. At this stage, the level-set defined in the coarse mesh is mapped to the new refined mesh by using standard interpolation of the element shape functions and the process is continued. The material properties n_1 or n_2 are assigned to elements of the mesh depending on whether they are at points with $\Psi_j(x) < 0$ (Si) or $\Psi_j(x) > 0$ (SiO_2). The elements eventually crossed by the phase interface (defined by $\Psi_j(x) = 0$) will have value n_1 by choice. Obviously, according to the above procedure, the resolution of the optimal material distribution depends directly on the fineness of the adopted mesh. The overall optimization procedure is conveniently summarized in pseudo-code format in Algorithm 1.

It is important to highlight that the topological derivative was specifically designed to deal with shape and topology optimization problems in which black/white solutions are required. In contrast to traditional topology optimization methods, the topological derivative formulation does not require a material model concept based on intermediary densities, so that interpolation schemes are unnecessary. These features are crucial in the design of nanophotonic devices, since the limitations arising from material model procedures are here naturally avoided. Specifically in this context, the decent direction $g(x)$ from (4.3) is continuous on the interface between Ω_1 and Ω_2 where the level-set function vanishes ($\Psi(x) = 0$), so that no any special treatment is needed. In addition, the topological derivative has the advantage of providing an analytical form for the topological sensitivity, which allows one to obtain the optimal design in a few iterations. Therefore, the resulting topology optimization procedure summarized through Algorithm 1 is remarkably efficient and of simple computational implementation, since it features only a minimal number of user-defined algorithmic parameters. On the other hand, with the algorithm being based on a gradient descent approach, it is not possible to make guarantees regarding the global optimality of any outcomes, which will depend upon the chosen initial guess. Nonetheless, the outcome is guaranteed to be a local optimum of the shape functional for a sufficiently refined mesh [19].

Algorithm 1: The topology design algorithm

Input: Ω, $\Psi_0, \epsilon_k, \epsilon_\theta$
Output: $\Omega^\star$

```
1  begin
2      j ← 0;
3      Ω_j ← Ψ_j;
4      compute the shape functional J(E) from (3.5);
5      compute the topological derivative D_T J(E) according to (3.6);
6      compute the steepest descent direction g from (4.2);
7      compute θ according to (4.4);
8      Ψ_old ← Ψ_j; J_old ← J(E); J_new ← 1 + J_old; k ← 1; θ_old ← θ;
9      while J_new > J_old do
10         compute Ψ_new according to (4.5);
11         Ψ_j ← Ψ_new;
12         execute lines 3 and 4;
13         J_new ← J(E);
14         k ← k/2;
15     end
16     if k < ε_k then
17         refine the mesh;
18         Ψ_{j+1} ← Ψ_j; j ← j + 1;
19         go to line 3;
20     else
21         if θ > ε_θ then
22             Ψ_{j+1} ← Ψ_j; j ← j + 1;
23             go to line 3;
24         else
25             return Ω* ← Ψ_j;
26         end
27     end
28 end
```

5. Numerical Experiments

In this section we present a set of numerical experiments showing different features of the proposed approach. The wavelength is given by $\lambda = 1.55\,\mu\text{m}$, which implies a frequency of 193.4 GHz. For each example, the refractive indices of Si and SiO_2 are set as $n_1 = 2.847$ and $n_2 = 1.444$, respectively. The silicon index represents an effective slab approximation for the 2D simulation of a 3D structure considering a 220 nm thick silicon layer surrounded by silicon dioxide and operating in the quasi-transverse electric mode [2]. For initial guess we consider the optimization domain Ω composed only by SiO_2 or only by Si. Since standard Galerkin method is used to discretize the BVPs, the finite elements mesh is constructed in such a way that the Ihlenburg-Babuška condition is fulfilled [20]. The PML layer has 1.0 µm of width. We also consider horizontal symmetry condition. Finally, we set $\epsilon_\theta = 1^\circ$ as the threshold for the numerical optimality condition. All numerical experiments were implemented in Matlab [21].

5.1. **Example 1.** In this example, the domain $\mathcal{B}$ is given by a rectangle of size 6.0 µm × 4.5 µm. The optimization domain Ω is given by a square of size 2.5 µm × 2.5 µm, centred

at the point $(3.75, 0)$. The waveguide has 0.45 µm of width and 2.5 µm of length. The source is given by

$$Q = \mathbf{i} \exp\left(-\frac{\|x\|^2}{0.01\lambda^2}\right) e_2, \tag{5.1}$$

where $\mathbf{i}$ is the complex unit, λ is the wave length and e_2 is the canonical basis vector in the vertical direction. Finally, the target domain ω is given by a circle with 272.2 nm of radius located at the center of Ω. See sketch in Figure 2.

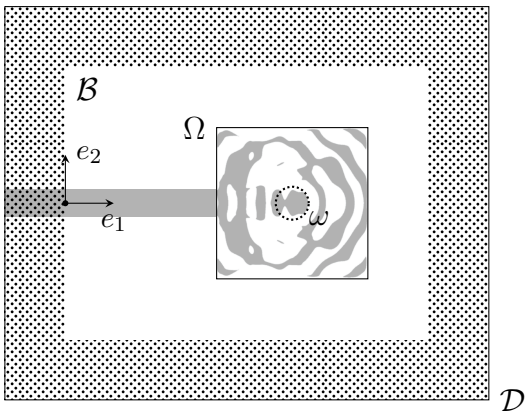

FIGURE 2. Example 1. The wave guide made of Si appears in grey, the SiO_2 is represented by the white region and the PML is patterned. The black dot represents the pole of the Gaussian source distribution and the target ω is represented by a dotted circle.

We start by setting $\Psi_0 = 1$ as initial guess (SiO_2). The energy density distributions are presented in Figures 3(a) and 3(b) for the initial and final configurations, respectively. The optimality condition has been reached at iteration 27, and the obtained topology is shown in Figure 4. The topology shows interesting features that resemble a resonator surounded by a dielectric grating, which is a traditional reflective structure created by alternating layers of two dielectric materials. At the same time, on the input side, the structure seems to partially change in order to favor the energy transport from the waveguide to the ω region through a segmented waveguide (waveguide/grating hybrid).

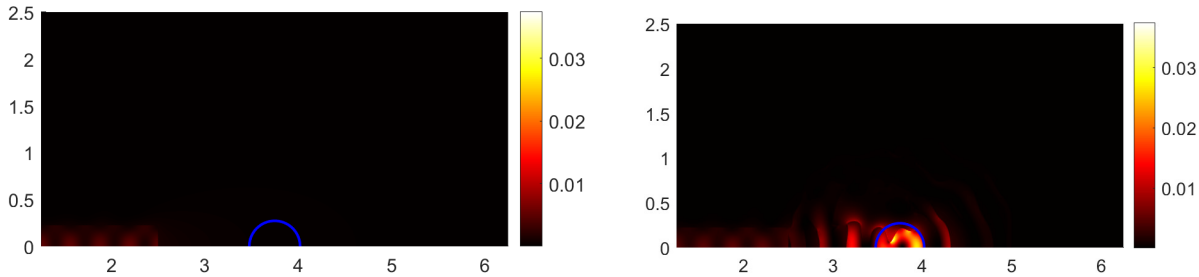

(a) initial energy density (b) final energy density

FIGURE 3. Example 1. Initial guess given by SiO_2: Energy density distributions. The target domain ω follows highlighted in solid blue line.

Now we consider $\Psi_0 = -1$ as initial guess (Si). Figures 5(a) and 5(b) show the initial and final energy density distributions, respectively. The resulting topology is presented in Figure 6, which shares many features with the previous result despite the opposite initial guess.

FIGURE 4. Example 1. Initial guess given by SiO_2: Resulting topology mirrored horizontally.

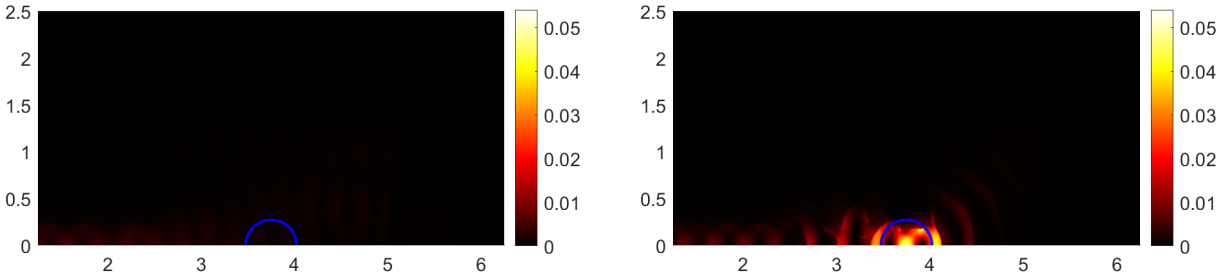

(a) initial energy density (b) final energy density

FIGURE 5. Example 1. Initial guess given by Si: Energy density distributions. The target domain ω follows highlighted in solid blue line.

FIGURE 6. Example 1. Initial guess given by Si: Resulting topology mirrored horizontally.

Finally, the histories of the angle θ and the energy evaluated in ω during the iterative process for both examples are presented in Figure 7, where we can see that the optimality

condition, in this case, has been reached at iteration 24. Table 1 shows a summary of the obtained results, including the number of iterations and the final energy evaluated in ω for the two experiments, with the result for the first only 23% below the second.

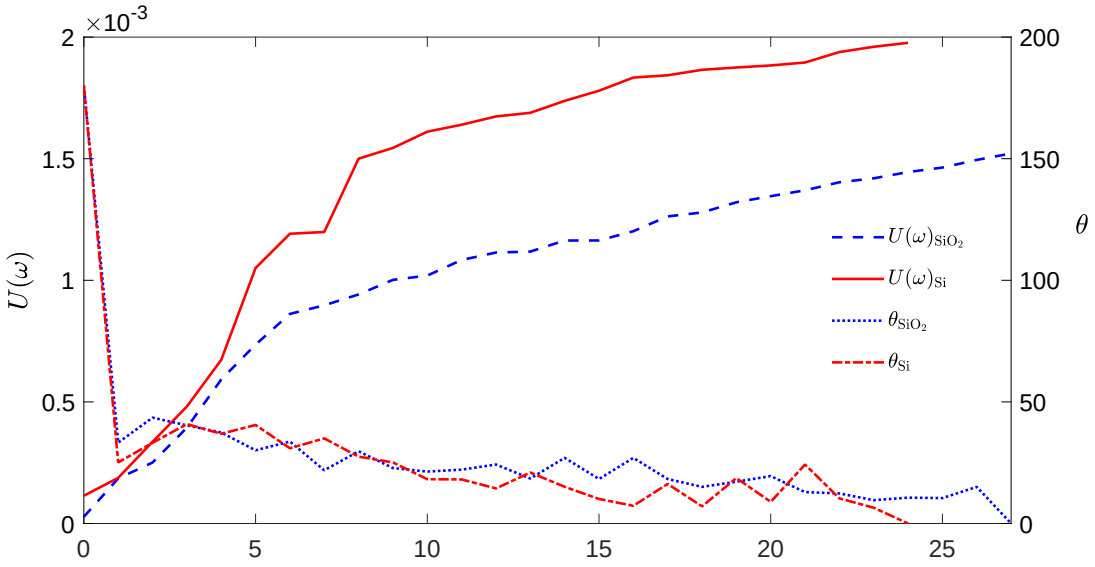

FIGURE 7. Example 1. Histories of the angle θ and energy evaluated in ω during the iterative process.

TABLE 1. Example 1. Number of iterations and final obtained energy evaluated in ω.

Ψ_0	# iterations	$U(\omega)$
$+1$	27	1.5215×10^{-3}
-1	24	1.9764×10^{-3}

5.2. **Example 2.** In this example, the domain $\mathcal{B}$ is given by a rectangle of size 7.1 µm × 4.5 µm. The optimization domain Ω is given by a square of size 2.5 µm × 2.5 µm, centred at the point $(3.85, 0)$. The waveguide has 0.5 µm of width and 4.0 µm of length, divided in two parts as shown in Figure 8. The source Q is uniformly distributed over the vertical line Γ of height $h = 0.4$ µm and centre at $(0.6, 0)$, namely

$$Q = \mathbf{i}\delta_\Gamma e_2, \tag{5.2}$$

where $\mathbf{i}$ is the complex unit, e_2 is the canonical basis vector in the vertical direction and δ_Γ is used to denote the Dirac delta-function concentrated on Γ. Finally, the target domain ω is given by a circle with 272.2 nm of radius located at the center of Ω. See again Sketch in Figure 8.

We start by setting $\Psi_0 = -1$ as initial guess (Si). The initial and final energy density distributions for this example are shown in Figures 9(a) and 9(b), respectively. The resulting topology is presented in Figure 10. The optimality condition has been reached at iteration 6.

It is interesting to note that the existence of a second waveguide to the right of the domain does not change the resulting topology significantly when compared to the first examples: we can still identify a grating-like structure to the right of ω and a hybrid waveguide/grating to the left. In practice, the grating structure isolates the region ω from

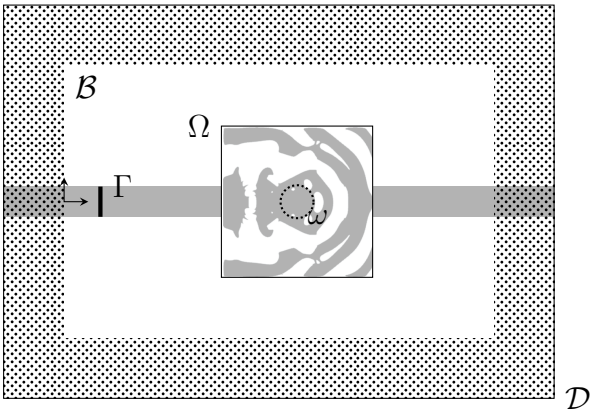

FIGURE 8. Example 2. The wave guide made of Si appears in grey, the SiO_2 is represented by the white region and the PML is patterned. The vertical line in black represents the region Γ where the source Q is uniformly distributed and the target ω is represented by a dotted circle.

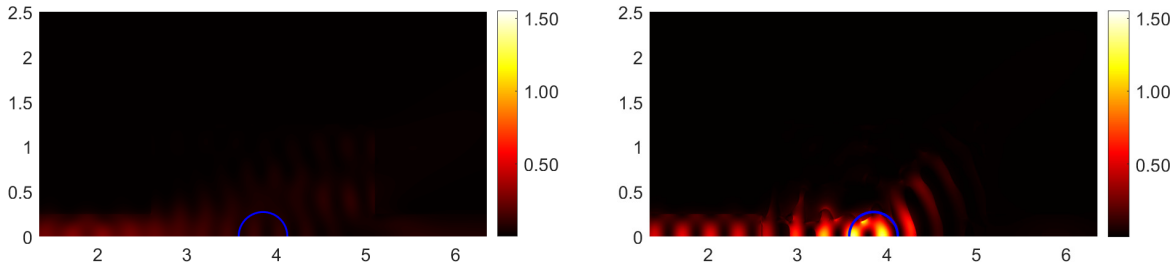

(a) initial energy density (b) final energy density

FIGURE 9. Example 2. Initial guess given by Si: Energy density distributions. The target domain ω follows highlighted in solid blue line.

FIGURE 10. Example 2. Initial guess given by Si: Resulting topology mirrored horizontally.

the second waveguide, as can be seen in the energy density distribution in Figure 9(b), justifying the little impact it has in the final topology.

It is well known that there is a lack of sufficient optimality conditions for such topology optimization problems [22], so that the final solution may strongly depend on the initial guess or any heuristic used in the minimization process. Therefore, in order to enforce the algorithm to land in some possible better local minimum, we impose a volume constraint of 25% over silicon material. Figure 11 and 12 show the final energy density distribution and the resulting topology. The optimality condition has been reached at iteration 21. By comparing Figures 9(b) and 11, we note a slice improvement on the obtained solution.

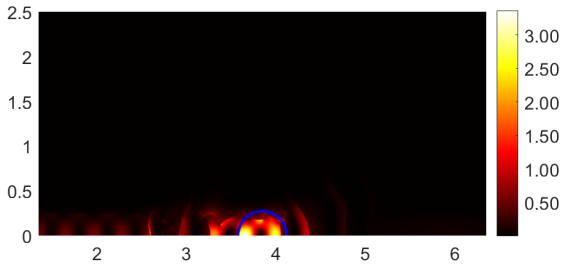

FIGURE 11. Example 2. Volume-constrained case: Final energy density distribution. The target domain ω follows highlighted in solid blue line.

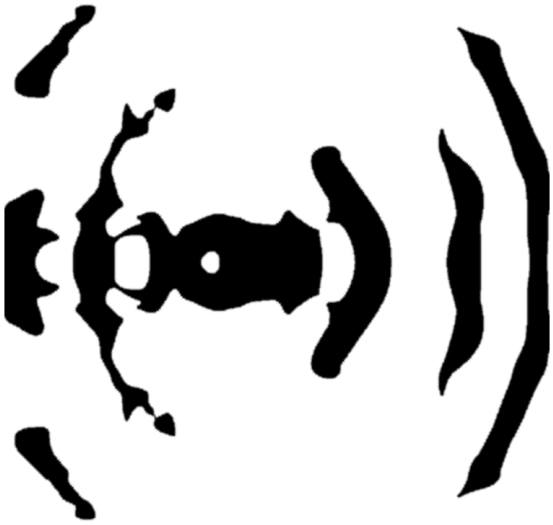

FIGURE 12. Example 2. Volume-constrained case: Resulting topology mirrored horizontally.

Now, we set $\Psi_0 = 1$ as initial guess (SiO_2). The energy density distributions are presented in Figures 13(a) and 13(b) for the initial and final configurations, respectively. The obtained topology is shown in Figure 14. The optimality condition has been reached after 20 iterations.

The histories of the angle θ and the energy evaluated in ω during the iterative process are presented in Figure 15. Finally, a summary of the obtained results is reported in Table 2, showing the number of iterations and the final obtained energy evaluated in ω for the three experiments. Together with the results from the first example, these results are an evidence of the abundance of local optima in the design of nanophotonic energy concentrators. This is indicative that the method should be successful even with the inclusion of further restrictions, such as fabrication constraints.

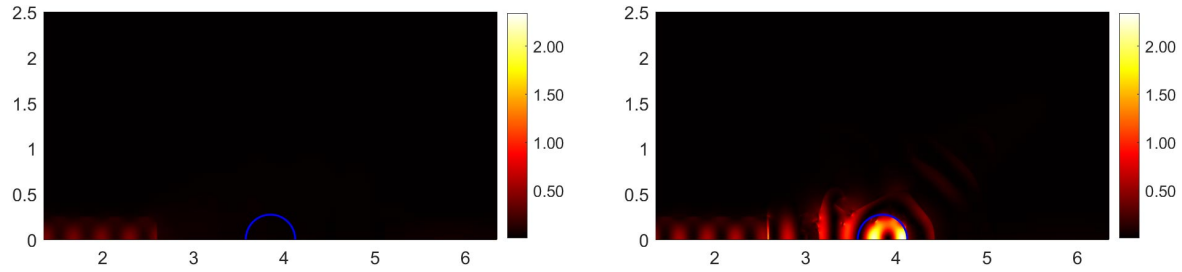

(a) initial energy density (b) final energy density

FIGURE 13. Example 2. Initial guess given by SiO_2: Energy density distributions. The target domain ω follows highlighted in solid blue line.

FIGURE 14. Example 2. Initial guess given by SiO_2: Resulting topology mirrored horizontally.

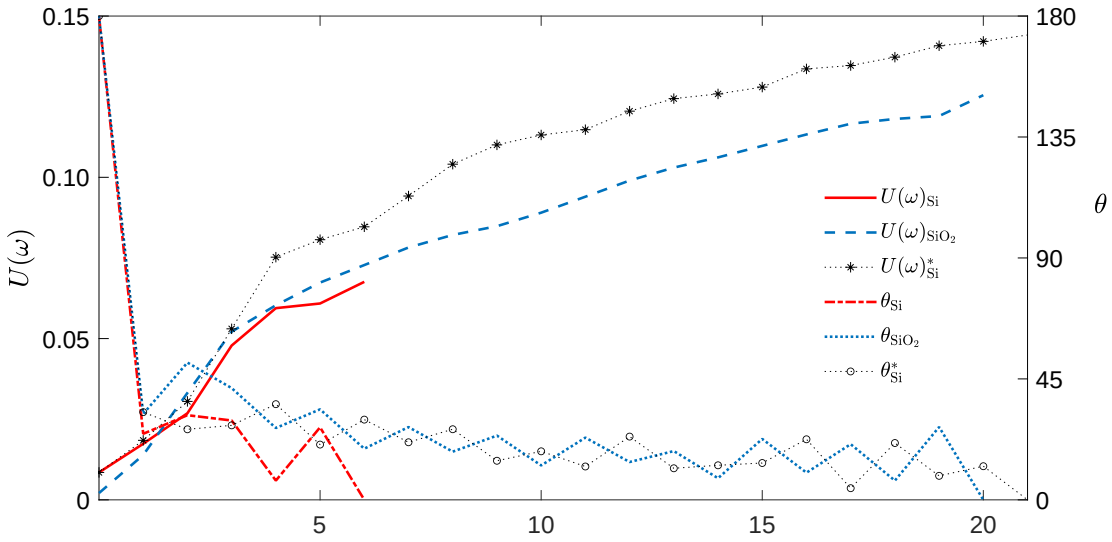

FIGURE 15. Example 2. Histories of the angle θ and energy evaluated in ω during the iterative process. *Volume-constrained case.

TABLE 2. Example 2. Number of iterations and final obtained energy evaluated in ω. *Volume-constrained case.

Ψ_0	# iterations	$U(\omega)$
-1	6	6.7590×10^{-2}
-1^*	21	1.4412×10^{-1}
$+1$	20	1.2546×10^{-1}

5.3. **Example 3.** In this example, the model problem is the same as the one described in Section 5.1, but the target domain ω is now given by two disjoints balls ω_1 and ω_2 according to the sketch in Figure 16.

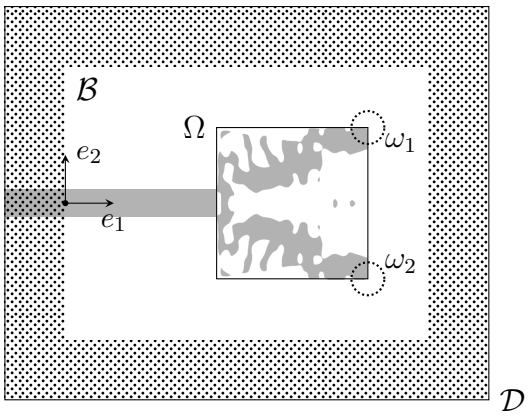

FIGURE 16. Example 3. The wave guide made of Si appears in grey, the SiO_2 is represented by the white region and the PML is patterned. The black dot represents the pole of the Gaussian source distribution and the target $\omega = \omega_1 \cup \omega_2$ is represented by two dotted circles.

We consider $\Psi_0 = -1$ as initial guess (Si). Figures 17(a) and 17(b) show the initial and final energy density distributions, respectively. The optimization process has stopped at iteration 89 with $\theta = 6.8°$, and the resulting topology is presented in Figure 18. In particular, the history of the energy evaluated in ω during the iterative process is presented in Figure 19.

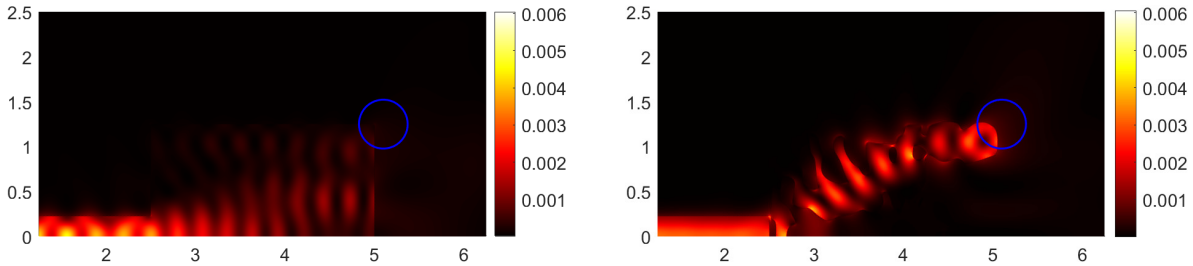

(a) initial energy density (b) final energy density

FIGURE 17. Example 3. Initial guess given by Si: Energy density distributions. The target domain ω follows highlighted in solid blue line.

In this case, the final topology shows interesting features that depart from the previous ones. Because the energy concentration regions are at the edge and partially outside the optimization domain, we do not see the same grating-like reflectors as clearly as before. On the other hand, the guiding structures are more pronounced, seen as they must guide

FIGURE 18. Example 3. Initial guess given by Si: Resulting topology mirrored horizontally.

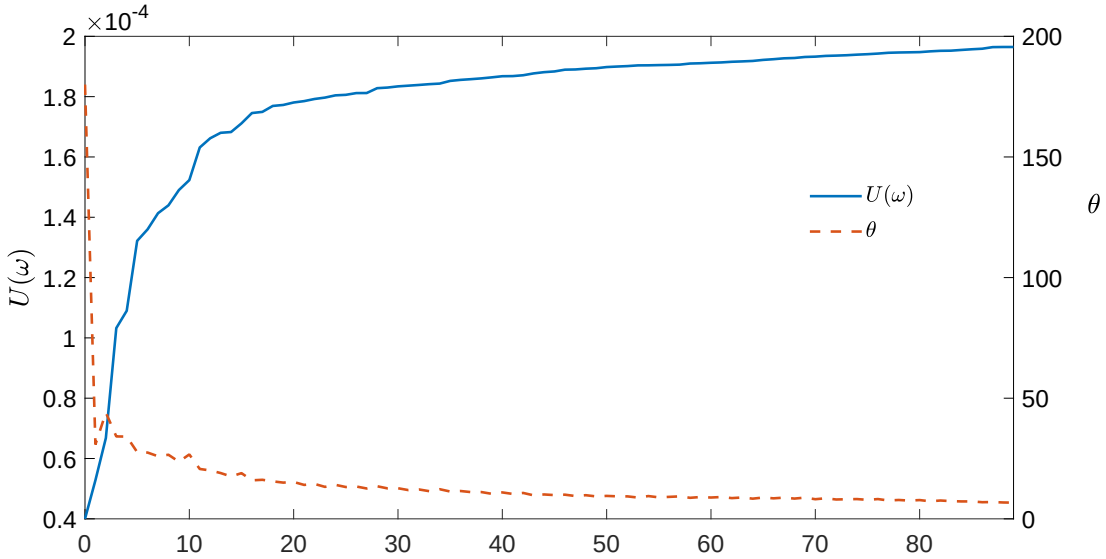

FIGURE 19. Example 3. History of the energy evaluated in ω during the iterative process.

the incoming light through a curved path. Furthermore, the initial portion of the structure seems to act as a power splitter, dividing the input power among both target regions.

6. Conclusions

In this paper, a novel approach for topology design optimization of nanophotonic device has been proposed. The forward problem is governed by Maxwell's equations in the frequency domain. The central idea consists in maximizing the electric energy within a small region of the nanodevice, with respect to the Si and SiO_2 spatial distribution. The topological asymptotic expansion of the shape functional, with respect to the nucleation of a small inclusion endowed with different material property from the back ground, has been rigorously derived. The resulting topological derivative has been used to devise a topology design algorithm based on a level-set domain representation method. Finally, a number of numerical experiments has been presented, showing different features of the

proposed approach, including its capability in producing energy-density hot-spots within the target domain, allowing to maximize the energy in these regions, as expected. In practice, fabrication constrains have to be considered together with design of the nano structures to enable manufacturing using current lithography technology, so that further developments are still required.

Acknowledgements

This study was financed in part by the Coordenação de Aperfeiçoamento de Pessoal de Nível Superior – Brasil (CAPES) – finance code 88881.311020/2018, CNPq (Brazilian Research Council) grant 302036/2018-0, FAPERJ (Research Foundation of the State of Rio de Janeiro), and São Paulo Research Foundation (FAPESP) grants 2015/24517-8, 2016/19270-6 and 2018/25339-4.

Appendix A. Proof of the main result

In this appendix, the proof of the main result of the paper reported in Theorem 1 is presented. Following the topological derivative method, let us introduce a topological perturbation confined in a small region $B_\epsilon(x_0) \subset \Omega$ of size ϵ and center at $x_0 \in \Omega$ of the form

$$\gamma_\epsilon(x) = \begin{cases} \gamma(x), & x \in B_\epsilon(x_0), \\ 1, & \text{otherwise} \end{cases} \tag{A.1}$$

where $\gamma(x)$ is defined in (3.4). Then the topologically perturbed counterpart of problem (2.1) is stated as: Find $E_\epsilon \in \mathcal{V}$ such that

$$\int_{\mathcal{D}} \left(\nabla \times E_\epsilon \cdot \nabla \times W - \gamma_\epsilon^2 k_0^2 n^2 E_\epsilon \cdot W \right) dx = \int_{\mathcal{D}} Q \cdot W \mathrm{d}x, \quad \forall W \in \mathcal{V}. \tag{A.2}$$

From these elements, we can state an auxiliary result concerning the existence of the topological derivative for the problem we are dealing with.

Lemma 3. *Let E and E_ϵ be the solutions of the variational problems* (2.1) *and* (A.2)*, respectively. Then, the following a priori estimate holds true:*

$$\|\tilde{E}_\epsilon\|_{H_{\mathrm{curl}}(\mathcal{D};\mathbb{C}^d)} \leq C \epsilon^{\frac{d}{2}+\delta}, \tag{A.3}$$

where C is a constant independent of the small parameter ϵ and $0 < \delta < 1$.

Proof. The proof of this result can be found in [12]. □

Hence, the perturbed counterpart of the electric energy defined in (2.4) is given by:

$$U_\epsilon(\omega) = \int_\omega k_0^2 n^2 \|E_\epsilon\|^2 \mathrm{d}x + \int_{B_\epsilon} (\gamma^2 - 1) k_0^2 n^2 \|E_\epsilon\|^2 \chi_\omega \mathrm{d}x, \tag{A.4}$$

where χ_ω is the characteristic function of the region ω. The solution $E_\epsilon \in \mathcal{V}$ to the variational problem (A.2) can be decomposed as

$$E_\epsilon = E + \tilde{E}_\epsilon. \tag{A.5}$$

By replacing (A.5) into (A.4), we obtain:

$$U_\epsilon(\omega) - U(\omega) = \int_{B_\epsilon} (\gamma^2 - 1) k_0^2 n^2 \|E\|^2 \chi_\omega + 2 \int_\omega k_0^2 n^2 \Re\{\overline{E} \cdot \tilde{E}_\epsilon\} \mathrm{d}x + \sum_{i=1}^{2} \mathcal{E}_i(\epsilon), \tag{A.6}$$

where

$$\mathcal{E}_1(\epsilon) = \int_\omega k_0^2 n^2 \|\tilde{E}_\epsilon\|^2 \mathrm{d}x, \tag{A.7}$$

$$\mathcal{E}_2(\epsilon) = \int_{B_\epsilon} (\gamma^2 - 1) k_0^2 n^2 (2\Re\{\overline{E} \cdot \tilde{E}_\epsilon\} + \|\tilde{E}_\epsilon\|^2) \chi_\omega \mathrm{d}x. \tag{A.8}$$

The above remainders can be bound by using Lemma 3 as follows:

$$|\mathcal{E}_1(\epsilon)| \leq \|\tilde{E}_\epsilon\|^2_{H_{\mathrm{curl}}(\mathcal{D};\mathbb{C}^d)} \leq C\epsilon^{d+2\delta} = o(\epsilon^d), \tag{A.9}$$

$$|\mathcal{E}_2(\epsilon)| \leq C\epsilon^{\frac{d}{2}} \|\tilde{E}_\epsilon\|_{L^2(B_\epsilon;\mathbb{C}^d)} \leq C\epsilon^{\frac{d}{2}+\delta} \|\tilde{E}_\epsilon\|_{H_{\mathrm{curl}}(\mathcal{D};\mathbb{C}^d)} \leq C\epsilon^{d+\delta} = o(\epsilon^d). \tag{A.10}$$

We can rewrite (A.2) by using the definition for the contrast (A.1) in the following form

$$\int_{\mathcal{D}} (\nabla \times E_\epsilon \cdot \nabla \times W - k_0^2 n^2 E_\epsilon \cdot W) \mathrm{d}x = \int_{B_\epsilon} (\gamma^2 - 1) k_0^2 n^2 E_\epsilon \cdot W \mathrm{d}x + \int_{\mathcal{D}} Q \cdot W \mathrm{d}x. \tag{A.11}$$

Then, after subtracting (2.1) from (A.11) we obtain

$$\int_{\mathcal{D}} (\nabla \times \tilde{E}_\epsilon \cdot \nabla \times W - k_0^2 n^2 \tilde{E}_\epsilon \cdot W) \mathrm{d}x = \int_{B_\epsilon} (\gamma^2 - 1) k_0^2 n^2 E_\epsilon \cdot W \mathrm{d}x. \tag{A.12}$$

Now by setting $W = \tilde{E}_\epsilon$ in (3.3) and $W = V$ in (A.12) we have

$$\int_{\mathcal{D}} (\nabla \times \tilde{E}_\epsilon \cdot \nabla \times V - k_0^2 n^2 \tilde{E}_\epsilon \cdot V) \mathrm{d}x = 2 \int_\omega k_0^2 n^2 \overline{E} \cdot \tilde{E}_\epsilon \mathrm{d}x \tag{A.13}$$

$$\int_{\mathcal{D}} (\nabla \times \tilde{E}_\epsilon \cdot \nabla \times V - k_0^2 n^2 \tilde{E}_\epsilon \cdot V) \mathrm{d}x = \int_{B_\epsilon} (\gamma^2 - 1) k_0^2 n^2 E_\epsilon \cdot V \mathrm{d}x. \tag{A.14}$$

From the symmetry of both bilinear forms and after taking the real part of the above equalities, the following important result holds true:

$$\int_{B_\epsilon} (\gamma^2 - 1) k_0^2 n^2 \Re\{E_\epsilon \cdot V\} \mathrm{d}x = 2 \int_\omega k_0^2 n^2 \Re\{\overline{E} \cdot \tilde{E}_\epsilon\} \mathrm{d}x. \tag{A.15}$$

Therefore, we can rewrite (A.6) as

$$U_\epsilon(\omega) - U(\omega) = \int_{B_\epsilon} (\gamma^2 - 1) k_0^2 n^2 \|E\|^2 \chi_\omega \mathrm{d}x + \int_{B_\epsilon} (\gamma^2 - 1) k_0^2 n^2 \Re\{E_\epsilon \cdot V\} \mathrm{d}x + \sum_{i=1}^{2} \mathcal{E}_i(\epsilon). \tag{A.16}$$

After replacing E_ϵ by $E + \tilde{E}_\epsilon$ according to (A.5), we obtain

$$U_\epsilon(\omega) - U(\omega) = \int_{B_\epsilon} ((\gamma^2 - 1) k_0^2 n^2 \|E\|^2 \chi_\omega)(x_0) \mathrm{d}x + \int_{B_\epsilon} ((\gamma^2 - 1) k_0^2 n^2 \Re\{E \cdot V\})(x_0) \mathrm{d}x + \sum_{i=1}^{5} \mathcal{E}_i(\epsilon), \tag{A.17}$$

where

$$\mathcal{E}_3(\epsilon) = \int_{B_\epsilon} (\gamma^2 - 1) k_0^2 n^2 \Re\{\tilde{E}_\epsilon \cdot V\} \mathrm{d}x \tag{A.18}$$

$$\mathcal{E}_4(\epsilon) = \int_{B_\epsilon} [((\gamma^2 - 1) k_0^2 n^2 E \cdot V)(x) - ((\gamma^2 - 1) k_0^2 n^2 \Re\{E \cdot V\})(x_0)] \mathrm{d}x \tag{A.19}$$

$$\mathcal{E}_5(\epsilon) = \int_{B_\epsilon} [((\gamma^2 - 1) k_0^2 n^2 \|E\|^2 \chi_\omega)(x) - ((\gamma^2 - 1) k_0^2 n^2 \|E\|^2 \chi_\omega)(x_0)] \mathrm{d}x \tag{A.20}$$

Now, we can bound the remainders (A.18)–(A.20) as follows. By using Lemma 3, the remainder $\mathcal{E}_3(\epsilon)$ can be bound as

$$|\mathcal{E}_3(\epsilon)| \leq C\epsilon^{\frac{d}{2}}\|\tilde{E}_\epsilon\|_{L^2(B_\epsilon;\mathbb{C}^d)} \leq C\epsilon^{\frac{d}{2}+\delta}\|\tilde{E}_\epsilon\|_{H_{\mathrm{curl}}(\mathcal{D};\mathbb{C}^d)} \leq C\epsilon^{d+\delta} = o(\epsilon^d). \tag{A.21}$$

From the Cauchy-Schwartz inequality and by taking into account the interior elliptic regularity of functions E and V, the remainders $\mathcal{E}_4(\epsilon)$ and $\mathcal{E}_5(\epsilon)$ are bounded as

$$|\mathcal{E}_4(\epsilon)| \leq C\epsilon^{d+1} = o(\epsilon^d) \tag{A.22}$$

$$|\mathcal{E}_5(\epsilon)| \leq C\epsilon^{d+1} = o(\epsilon^d) \tag{A.23}$$

Finally, the topological asymptotic expansion of $U_\epsilon(\omega)$ is written as follows:

$$U_\epsilon(\omega) - U(\omega) = |B_\epsilon|(\gamma^2 - 1)k_0^2 n^2(\|E\|^2\chi_\omega + \Re\{E \cdot V\})(x_0) + o(\epsilon^d), \tag{A.24}$$

which allows for promptly identifying the leading term of order $O(\epsilon^d)$.

References

[1] Nanotechnology examples and applications. https://www.nanowerk.com/nanotechnology-examples-and-applications.php. Accessed: 2021-04-14.

[2] Donald L. Lee. *Electromagnetic Principles of Integrated Optics*. Wiley, New York, 1986.

[3] Lukas Chrostowski and Michael Hochberg. *Silicon Photonics Design*. Cambridge University Press, Cambridge, 2015.

[4] Martin Philip Bendsøe and Noboru Kikuchi. Generating optimal topologies in structural design using a homogenization method. *Computer methods in applied mechanics and engineering*, 71(2):197–224, 1988.

[5] Martin Philip Bendsoe and Ole Sigmund. *Topology optimization: theory, methods, and applications*. Springer Science & Business Media, 2013.

[6] Zejie Yu, Haoran Cui, and Xiankai Sun. Genetic-algorithm-optimized wideband on-chip polarization rotator with an ultrasmall footprint. *Optics letters*, 42(16):3093–3096, 2017.

[7] Salim Boutami and Shanhui Fan. Efficient pixel-by-pixel optimization of photonic devices utilizing the dyson's equation in a green's function formalism: Part i. implementation with the method of discrete dipole approximation. *JOSA B*, 36(9):2378–2386, 2019.

[8] Nicolas Lebbe, Alain Glière, Karim Hassan, Charles Dapogny, and Edouard Oudet. Shape optimization for the design of passive mid-infrared photonic components. *Optical and Quantum Electronics*, 51(5):1–14, 2019.

[9] Lin Xu and Huanyang Chen. Conformal transformation optics. *Nature Photonics*, 9(1):15–23, 2015.

[10] Jakob Søndergaard Jensen and Ole Sigmund. Topology optimization for nano-photonics. *Laser & Photonics Reviews*, 5(2):308–321, 2011.

[11] Sean Molesky, Zin Lin, Alexander Y Piggott, Weiliang Jin, Jelena Vucković, and Alejandro W Rodriguez. Inverse design in nanophotonics. *Nature Photonics*, 12(11):659–670, 2018.

[12] J. L. P. Ruiz, A. A. S. Amad, L. H. Gabrielli, and A. A. Novotny. Optimization of the electromagnetic scattering problem based on the topological derivative method. *Optics Express*, 27(23):33586–33605, 2019.

[13] J. Sokołowski and A. Żochowski. On the topological derivative in shape optimization. *SIAM Journal on Control and Optimization*, 37(4):1251–1272, 1999.

[14] A. A. Novotny and J. Sokołowski. *Topological derivatives in shape optimization*. Interaction of Mechanics and Mathematics. Springer-Verlag, Berlin, Heidelberg, 2013.

[15] A. A. Novotny and J. Sokołowski. *An introduction to the topological derivative method*. Springer Briefs in Mathematics. Springer Nature Switzerland, 2020.

[16] A. A. Novotny, J. Sokołowski, and A. Żochowski. *Applications of the topological derivative method*. Studies in Systems, Decision and Control. Springer Nature Switzerland, 2019.

[17] Xiangdong Liang and Steven G. Johnson. Formulation for scalable optimization of microcavities via the frequency-averaged local density of states. *Optics Express*, 21(25):30812, December 2013.

[18] S. Amstutz and H. Andrä. A new algorithm for topology optimization using a level-set method. *Journal of Computational Physics*, 216(2):573–588, 2006.

[19] S. Amstutz. Analysis of a level set method for topology optimization. *Optimization Methods and Software*, 26(4-5):555–573, 2011.

[20] F. Ihlenburg and I. Babuška. Finite element solution of the Helmholtz equation with high wave number part i: The h-version of the FEM. *Computers & Mathematics with Applications*, 30(9):9–37, 1995.

[21] MATLAB. *version 9.7.0.1216025 (R2019b) Update 1*. The MathWorks Inc., Natick, Massachusetts, 2019.

[22] S. Amstutz and N. Van Goethem. Topology optimization methods with gradient-free perimeter approximation. *Interfaces and Free Boundaries*, 14(3):401–430, 2012.

(R. Mattoso, A.A. Novotny*) Laboratório Nacional de Computação Científica LNCC/MCT, Coordenação de Métodos Matemáticos e Computacionais, Av. Getúlio Vargas 333, 25651-075 Petrópolis - RJ, Brasil

Email address, *Corresponding author: novotny@lncc.br

(L.H. Gabrielli) Photonics Research Center, School of Electrical and Computer Engineering, University of Campinas, Campinas - SP, Brazil

Email address: lhg28@unicamp.br